Supplement.

S1. Size distributions

We have identified a "leading edge" of the size distribution which is "leading" in terms of particle growth.   This "leading edge" terminology refers to the large-particles at the leading edge of the distribution and here we clarify this further. This is beyond what one would naturally think of as the leading edge particularly as we fit lognormals to this data which requires to some extent data on both sides of a peak. So in terms of the fit, data should extend from the "leading edge" at the far right all the way down in size to the inflection point between the large particle peak and the minimum towards smaller sizes. Note that N_p is for "large particles" that are defined differently: all those with D_p >= 2.4 nm. It is important to maintain the distinction of which criterion was used to derive any particular parameter (e.g. D_{le}, not D_p). In practice, the integration of the lognormal fit and N_p do not differ appreciably. Also some distributions do not exhibit an inflection point and were not able to be fit automatically. In these cases, lognormals were fitted by eye, using an average width from contemporary distributions. See section S2.x for examples.

A clear understanding of how two modes can be formed helps to explain the change in the size distribution exhibited in Fig. 2b. With decreasing amount of base contamination entering PhoFR over time, the region of base-stabilized nucleation at the top of the reactor shortens and nucleation cuts off sooner. Thus for given production of [SA], the earliest nucleated particles grow by the same amount (matching the right edges in Fig. 2b) but nucleation ceases earlier than less pure conditions so there are fewer particles on the trailing edge (left of peak) of the growing mode in Fig. 2b. The apparent size shift may not really be extra growth but just a drop in numbers on the trailing edge of the mode. Of course the interplay between these effects depends on what type of impurity is present and if there is more than one type or multiple sources.

S1.1 Modeled size distributions.

Shown below are model results for two runs, one without added base i.e., nucleation due to only the binary system as incorporated into that thermodynamics, and one with 400 pptv NH_3 added. HONO flow Q_4 = 2 sccm was simulated, and experimental measurements for no added base (nominal) and for 230 pptv NH_3 are shown in the two figures respectively.

The distributions change in expected ways along the length of the flow reactor. For example, in the binary system N_p (Dp > 2 nm, or cluster size > 10 SA molecules) increases dramatically with distance along the flow reactor and maximizes at the end of the reactor (120 cm).   For the added NH_3 case, however, the total number of particles is relatively constant in the lower half of the reactor. From 80 to 120 cm, the number of large particles increases by a factor of 20 in the binary case while in the added NH_3 case this number increases by a factor of only 1.4. The "large particles" in general grow larger as they flow down the reactor with this growth best exhibited in the added-NH_3 case with a nice progression in the peak towards large sizes in the distributions from 60 to 120 cm.
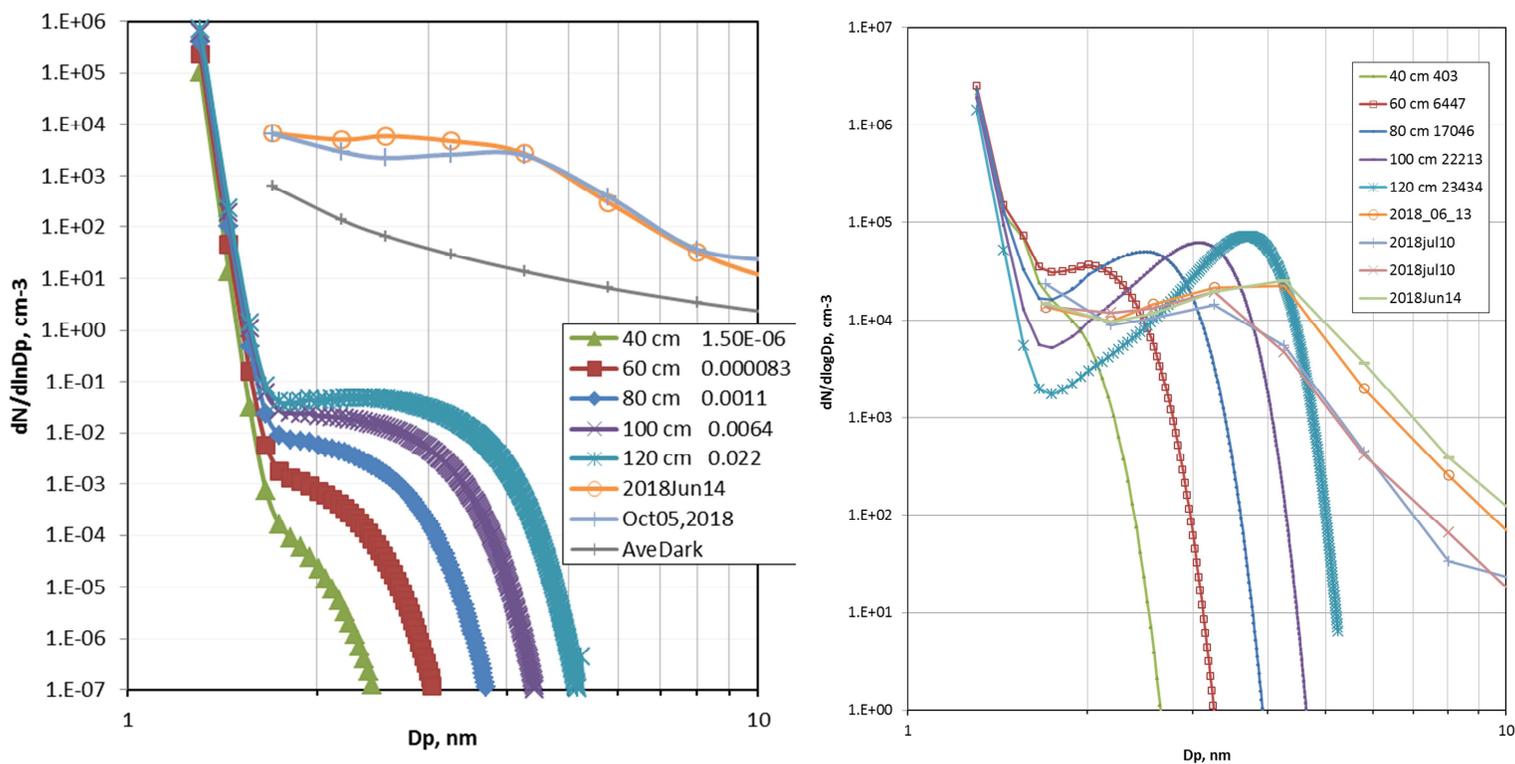
Fig. S1. (a) Binary simulations centerline concentrations and (b) 400 pptv NH3 added simulations. Shown in both plots are measured size distributions for no-added NH3 (left hand plot) and for 230 pptv NH3 added (right hand plot.)

The cluster scheme in the simulation (Hanson et al. 2017) only approximately captures the effects of coagulation and scavenging (i.e. particle-particle collisions): fully including these effects would decrease cluster concentrations and the predicted number of particles, possibly improving the comparison in Fig. S1(b).

The log-normal functions were fitted to the data for mobility diameters ≥ 2.4 nm to spotlight the properties of the largest particles, those that nucleated near the top of the flow reactor. Particles of intermediate size form along the length of the reactor and for some experiments (such as in Fig. 4b) they can be delineated from the other particles. Particles and clusters generated in this region are interesting but understanding them awaits further experimentation and more rigorous analytical tools. Here, we focus on the largest particles, those that are at the leading edge of the distributions. We attempt to isolate particles from one region of the flow reactor to better define the sulfuric acid which applies to that experiment.

S1.2 Multi-modes and size of large particle mode

Mode diameter data for Q_1 (SO_2 mixture) = 4 sccm and > 20 sccm are shown below. While the effects on Np (Fig. 2a) due to the addition in late February of the Teflon mesh near the top of PhoFR are very large,

the effects on mode diameter are noticeable (Fig. S2) but less pronounced. It is presumed that this mesh suppresses eddies in the cone from interacting with the cylindrical flow reactor region.

The leading edge mode of the size distributions were fit to log-normal functions using an Excel add-in (written in Visual Basic, "LgnFit.xlam", M. R. Stolzenburg, private communication).   The routine 'LgnFit' fits a log-normal to the upper half of a measured distribution, resulting in leading-edge parameters D_{le}, $\ln\sigma_{le}$ and $N_{p,le}$. Shown in Fig. S2 are a measured distribution and two lognormals, one using LgnFit and one that was manually fit to the leading edge particles. The fitting routine included the 4.3 nm data and thus resulted in a wider distribution. Which of the two lognormals is the best for interpreting the data may depend on what physical process is being probed. In terms of the size to which the largest particles can grow, the mode diameters of these lognormals are not significantly different.
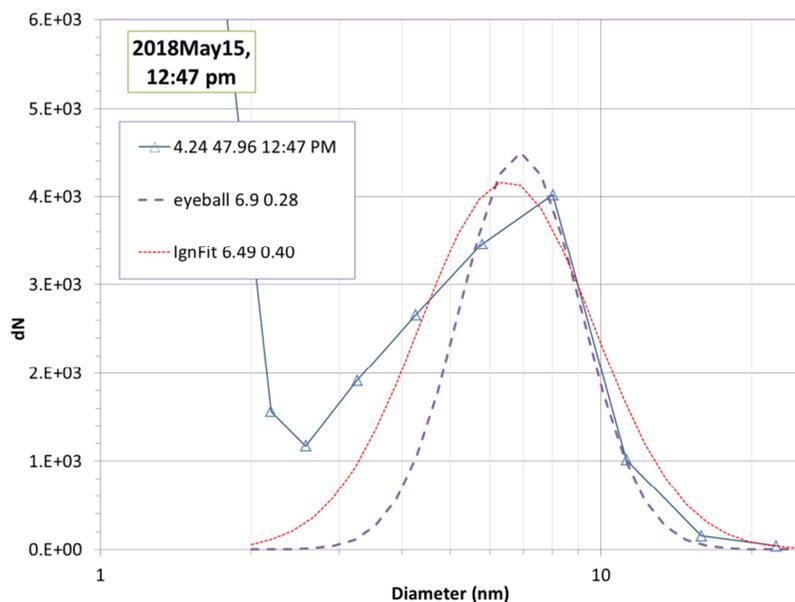
Fig. S2. Size distribution and two lognormals. Vertical axis is corrected concentrations.
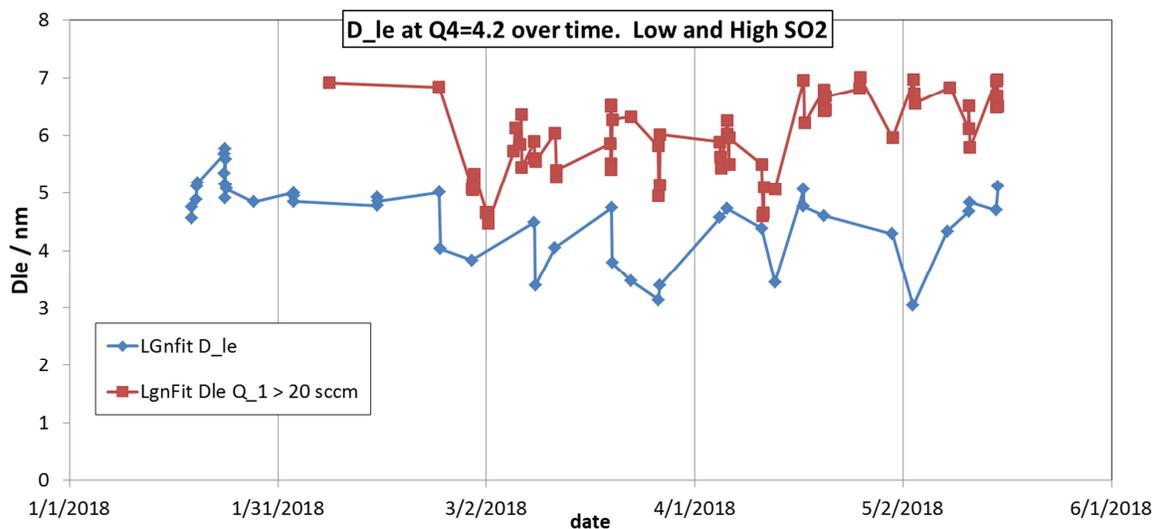
Fig. S3. Diameter of the leading-edge lognormal mode of the measured size distributions. High SO_2 data in red squares; low SO_2 are the blue diamonds.

S2. Historical PhoFR data

During the course of this study, the experimental apparatus was moved to a lab in a newly-constructed building. The gas source was switched from cleaned air (AADCO 737) to nitrogen from a liquid nitrogen gas-pack dewar (Airgas). This nitrogen is listed as having < 10 ppm oxygen impurity level, and apparently there is enough present as there was little effect on size distributions when oxygen was added. Data for typical baseline conditions for the year previous to this move are presented in Figs. S4.
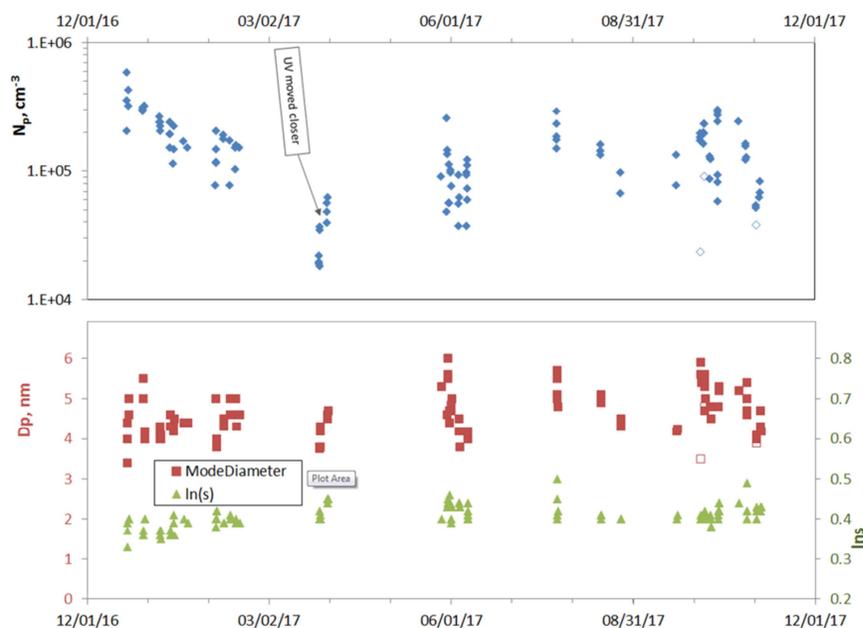
Figure S4(a,b) Data for typical conditions: 50 % RH, 296 K, total flow of 3 sLpm, Q_4=4.3 sccm and Q_{SO2mix}=4.1 sccm (the latter two result in HONO of 20 ppbv and SO_2 = 2 ppmv). (a) total particle number density, N_p, and (b) the mode diameter and lnσ as a function of time (from eyeball lognormals). See the discussion below and in Glasoe et al. for more information on the distributions at diameters <= 2 nm.

Over this time period, N_p averages about 1×10^5 cm^{-3}, the mode diameter has an average of about 5 nm, and the majority of the lnσ values are between 0.4 and 0.44. Since late March 2017, when the UV lights were moved a few cm closer to the flow reactor, trends in the data with time are not evident although the scatter remains significant. Three recent data points are not filled in and they were taken just before the NaONO(s) powder was lightly shaken. It is noteworthy that this process makes a difference however the effect is variable, e.g. in early November the NaONO vessel was shaken and the N_p increase was only about 25 %, less than the +100 %/-50 % day-to-day variability. The causes of this variability have not been identified but temperature variations are a likely cause, that of the room as well as that of the HCl-source.

S3. Experiments with added NH$_3$: sizes and distributions.

When NH$_3$ is added to PhoFR, the leading-edge particles of the size distributions become very well-defined. This is also true for the measurements presented in Glasoe et al., but in that case the very low number of particles without the dilution system attached, less than 1 cm^{-3}, indicated a very clean flow reactor. The probable contaminant amine in the dilution system used in Glasoe et al. is a separate issue.

Shown in Fig. S4 are representative size distributions for the present measurements taken in PhoFR (2018Jun13) and for measurements in the Nucleation Flow Reactor (NFR) used by Glasoe et al.

(2013Jun27) along with a more recent measurement from that apparatus (2016_01_20). The size distribution from January 2016 is very narrow compared to the others and this is probably due to the 25 °C temperature of the mixing region and sulfuric acid reservoir (these were regulated at 35 °C for the Glasoe et al. data set.) Note that the abundance of H_2SO_4 is greatest near the top of NFR and drops by 2/3 or so as the particles travel to the detector: much different than the H_2SO_4 abundance in PhoFR (Fig. 3). There are fewer particles in the present measurements but they are able to grow to larger sizes due to their larger overall exposure to H_2SO_4 in PhoFR.
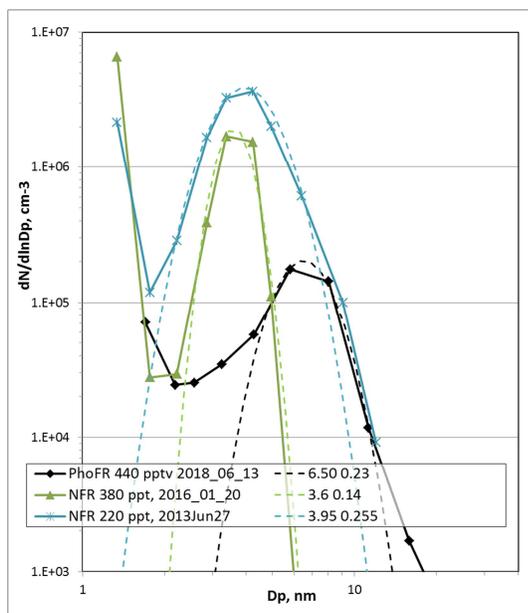
Fig. S4. Size distributions for PhoFR in comparison to those of NFR. NFR is the bulk-source flow reactor of Glasoe et al. 2014 with flows set such that [H2SO4] is about $4x10^9$ cm^{-3} where particles form. The 220 pptv NH_3 data is from Glasoe et al. while the 2016 data with 380 pptv NH_3 was taken with the bulk source held at a lower temperature (25 C vs. 35 C for Glasoe et al.) PhoFR data at 440 pptv with Q4=4.2 sccm which is an [H_2SO_4] estimated to be $3x10^9$ cm^{-3} where nucleation occurs.

When NH_3 was added to PhoFR, lognormals from both the eyeball and LgnFit were affected. The leading-edge diameters increased and the widths decreased upon NH_3 addition. This is demonstrated in Fig. S5, plots of mode diameters vs. HONO level (Q_4) for two different amounts of added NH_3.
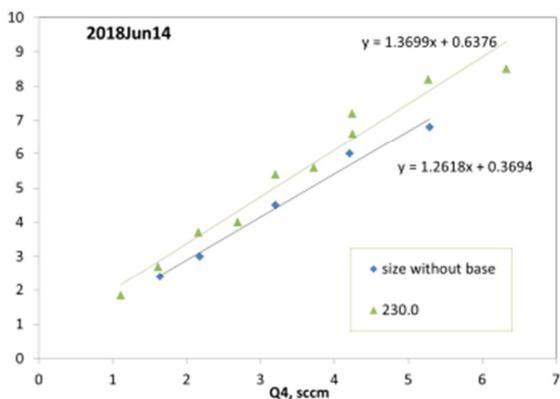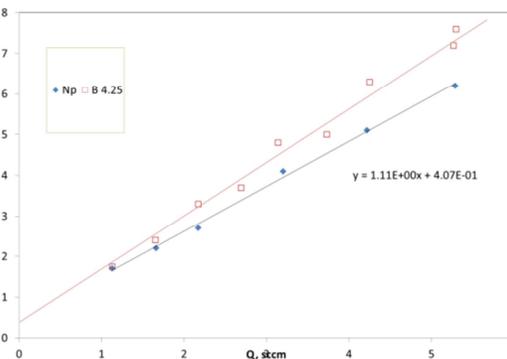
S4. Dark Counts.

At least daily, the UV lights were turned off to get a measure of the average dark counts. The count rate for these conditions was typically 0.05 s^{-1} but ranged as low as 0.02 s^{-1} and it was independent of

reactant concentrations. Note that corrections for losses and charging efficiency increase as particles get smaller, thus there is an increase in corrected dark counts towards smaller particles. They can significantly influence the fits at the lowest Q_4 values, introducing additional uncertainty in the log-normal fit parameters.

S5. Assessment of HONO level and photolysis rate.

S5.1 UV-Vis absorption experiment.

The HONO-containing flow was sent through a 1.05 m long absorption cell to assess the HONO level by absorption using a small diode array detector (Red Tide, Ocean Optics, ~ 3 nm resolution). The source was either a small UVA lamp or a white light. Shown in the figure are the transmissions for several measurements and the expected transmission for a HONO level of 20 ppmv (cross section from NASA data panel averaged over 4 nm). The absorptions for the two sources differ perhaps due to differences in scattered light within the instrument. There is a noticeable absorption at 400 nm and longer which can probably be assigned to NO2 (see absorption due to 5 ppmv, JPL1990 cross sections). Syomin and Finlayson-Pitts (2003) saw HONO decay of about 10 % in a 100 min in the presence of 50 % RH. The water content of gas flowing from the HONO source is about 76% RH at 20 C which may decrease to about 50 % at 23-25 C, the temperature of the absorption cell. Some loss of HONO and formation of NO_2 is expected but it is difficult to quantify to what extent from the previous work. It is also difficult to determine where this conversion may have happened.
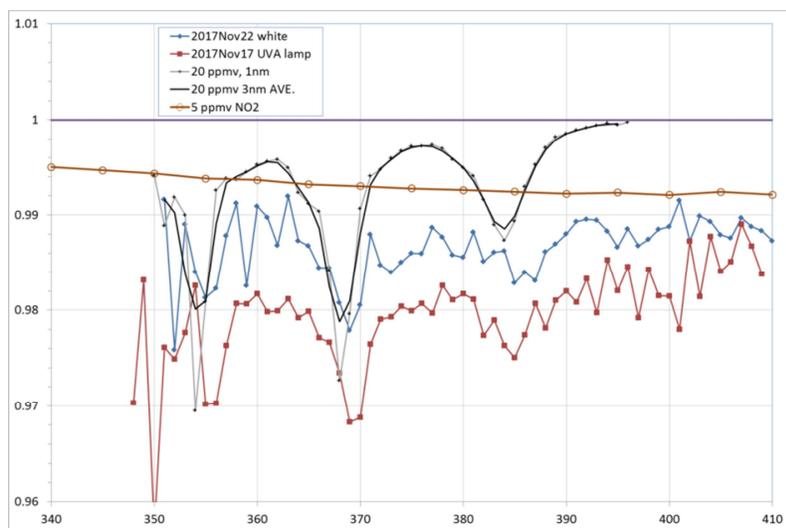
Fig. S6. Measured absorption spectra of HONO in the flow exiting the HONO generation system. Representative transmission spectra for 20 ppm HONO and 5 ppmv NO2 are also shown.

S5.2 PTrMS measurements of isoprene oxidation due to HONO photolysis.

The amount of OH-photolyte generated for typical conditions (Q_4=4.3 sccm, 3 sLpm total flow) was evaluated by adding isoprene to the flow and monitoring the amount of methyl vinyl ketone and methacrolein produced using a PTrMS system (Hanson et al.). An aliquot of isoprene in a diffusion tube, immersed in ice was teed into a flow entering PhoFR resulted in a level of isoprene = 6.6×10^{12} cm^{-3} as determined with the PTrMS (signal on mass 70 was used: the M.H+ signal at 69 u was too high to be well

quantified.) An increase in the signal at 71 u (M.H+ for MVK and MACR) of about 0.28 % of the signal due to isoprene was observed when the UV lights were turned on. Using a yield of 0.7 for these species (ref.) and a factor of 1.8 due to better detection of MVK+methacrolein vs. isoprene (ref.), a loss of about 0.22 % of the isoprene was due to reaction with OH. The signals are plotted vs. time in Fig. S
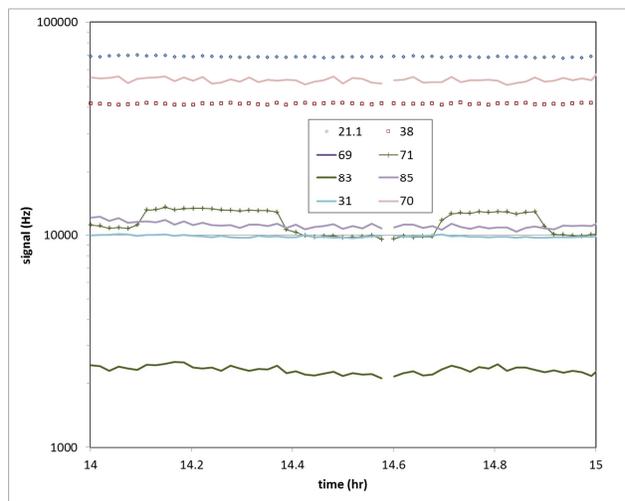
Fig. S7. Signals from PTrMS.

With a 33 s residence time, isoprene undergoes an average pseudo-first order loss rate coefficient of 6.7×10^{-5} s^{-1} (0.0022/33). Multiplying this by 6.6×10^{12} cm^{-3} results in an OH production rate of 4.4×10^{8} molecule cm^{-3} s^{-1}. Equating this to [HONO]*$k_{photolysis}$ and using 15 ppbv for the HONO mixing ratio, we arrive at a value for $k_{photolysis}$ of 0.0008 s^{-1}. In a second set of experiments, the total flow was halved keeping the HONO and isoprene source flows constant (thus doubling their abundance in PhoFR) resulted in an increase in the change in signal when turning on the UV lights for MVK + MACR (mass 71) that was about 4 times the change shown in the Figure. This result is consistent with expectations.

S6. Ammonia 'holdover'.

When the flow reactor was subjected to large exposures to ammonia, there was a large holdover and residual ammonia affected results for up to several days. This is shown in Fig. S8, a plot of Np vs. date on runs surrounding (red squares: no base added) days when runs with 2000 pptv NH$_3$ was added. Two days when this amount of NH$_3$ was added (blue diamonds) had N$_p$ that increased with time, by more than an order of magnitude.
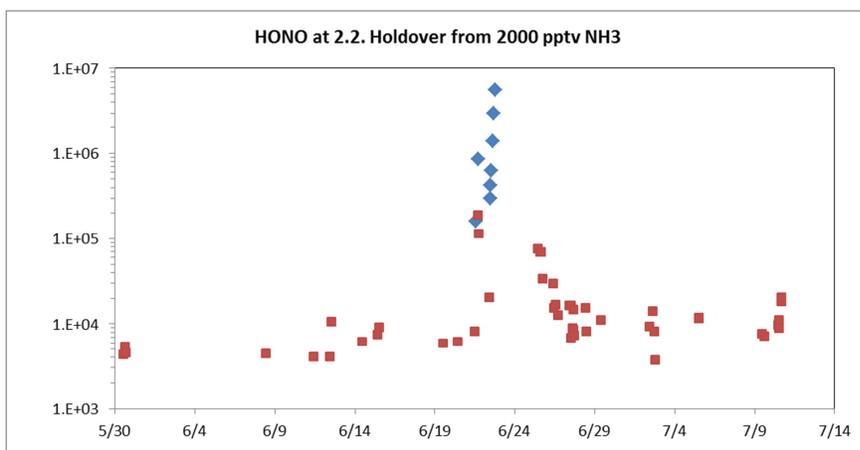
This amount of ammonia affected experimental conditions and the most likely effect is neutralization of the acid on the wall. This conditioning is presumably due to ammonium bi-sulfate formation on the walls, a decreased loss of NH$_3$ in that region, and more NH$_3$ is transported down the reactor where it can interact with the high SA levels found there. After each of the two additions, N$_p$ without added NH$_3$ was quite high and after the second run high N$_p$ persisted for several days.

S7. Model details.

The model is a 2D representation of the flow reactor and was built upon the model presented in Hanson et al. (2017), with details of acid-base clustering presented in the Supplement of that work. In addition to changes in the flow rate (2.9 sLpm here), the present simulations included the production of H_2SO_4 from the photolysis of HONO and subsequent oxidation of SO_2. The main inputs for the simulation are HONO and SO_2 levels, a 1st-order photolysis rate coefficient for HONO and the amount of base in the inlet. The photo-oxidation scheme and rate coefficients are shown in table S1. The flow rate was varied in the model from 2.8 to 3.0 and the large clusters (i.e., Np) were insensitive to flow rate. The number of acid molecules in the largest clusters in the simulation was varied from 6, 8, and 10, maintaining maximum NH_3-content to 3, and only small variations were observed in the concentration of the largest clusters (summing over base content). This was much in line with what we reported previously. Presented in S1 above were runs where clusters were allowed to grow to 250 sulfuric acid molecules. In this work, base was introduced into simulated 2D flow reactor uniformly distributed across the radius of the flow reactor.

Table S1. Photochemistry included in the simulation leading to the production of H_2SO_4. O_2 and H_2O are present in great abundance and were not simulated along with other transient species (O, $HOSO_2$, SO_3, HO_2SO_2.)

rxn no.	reactants				products			nomenclature and rate coefficient	unit or note
1	HONO	+	hv	→	OH	+	NO	kphot.= 8e-4 s^{-1}	s^{-1}
2	OH	+	SO_2	→	$HOSO_2$			k1x5 = 0.89e-12	cm^3/s
2'	O_2	+	$HOSO_2$	→	SO_3	+	HO_2	*prompt*	a
2''	SO_3	+	2 H_2O	→	H_2SO_4	+	H_2O	*prompt*	a
5a	OH	+	OH	→	H_2O	+	O	k1x1wo = 1.4e-12	cm^3/s
5b				→	H_2O_2			k1x1m = 6e-12	cm^3/s
6	OH	+	HO_2	→	H_2O	+	O_2	k1x3 = 1.1e-10	cm^3/s
7	OH	+	HONO	→	H_2O	+	NO_2	k1x7 = 6e-12	cm^3/s
8	OH	+	NO	→	HONO			k1x2 = 1e-11	cm^3/s
9	OH	+	NO_2	→	$HONO_2$			k1x6a = 1e-11	cm^3/s
9b	OH	+	NO_2	→	HOONO			k1x6b = 1.4e-12	cm^3/s
9b_r			HOONO	→	OH	+	NO_2	k_10 = 0.7	s^{-1}
10	HO_2	+	NO	→	HO	+	NO_2	k2x3 = 8.5e-12	cm^3/s
11	HO_2	+	NO_2	→	HO_2NO_2			k3x6 = 1.7e-12	
11_r			HO_2NO_2	→	HO2	+	NO2	k_4 = 0.11	s^{-1}
12	HO_2	+	HO_2	→	H_2O_2	+	O_2	k3x3 = 4.8e-12	b
13	HO_2	+	SO_2	→	HO_2SO_2			k3x5 = 3e-17	cm^3/s
14	{H_2O}	+	HO_2SO_2	→	H_2SO_4	+	{OH}	*prompt*	c

All rates from IUPAC or NASA-15 except 13, D. Davis et al. Species designations: 1, OH; 2: NO, 3: HO2, 4:HO2NO2, 5: SO2, 6: NO2, 7: HONO, 8: HNO3, 9: H2O2, 10: HOONO

a: Assumed to be very fast.   b: Includes water chaperone effect. c: Speculative rate and products: OH assumed to be produced.

Shown in Fig. S9 are variation of Np with HONO with the simulations including either NH_3 (70, 200 and 400 pptv) or DMA (5 ppqv). Experimental data for nominally-clean conditions and for 230 pptv NH3 added are shown also. The simulations with Nh3 in the range 70-200 pptv NH3 yield Np similar to the experimental and furthermore result in dependencies upon HONO that align with experimental results. The powerful nucleator DMA entering the flow reactor at 5 ppqv (1.2 $\times 10^5$ cm^{-3}) yields simulated N_p in the ballpark of the experimental N_p, its effect is limited at increasing HONO due to scavenging. These simulations suggest a potential contaminant is weaker than alkyl amines, perhaps ammonia or an amide.
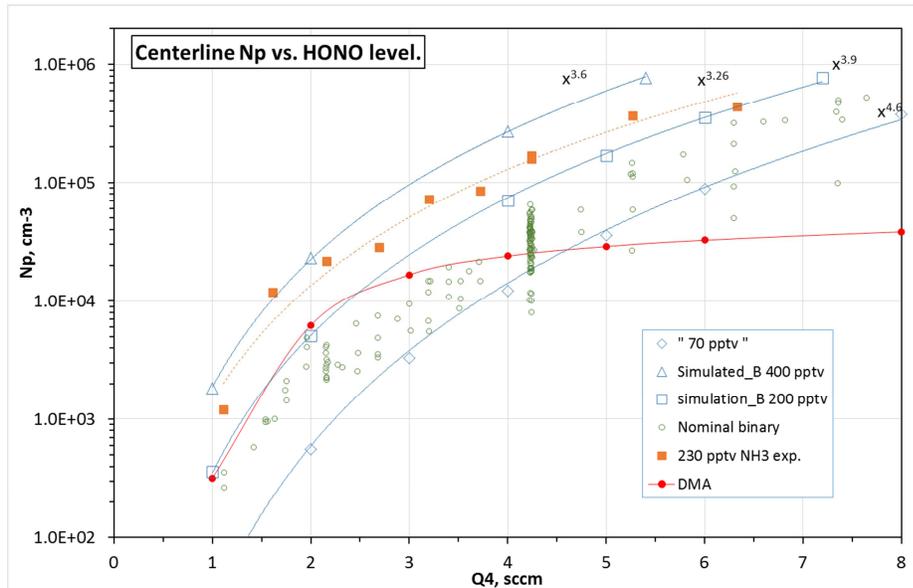
S8. Effect of SO_2.

Simulated H_2SO_4 profiles are sensitive to the value of this rate coefficient. Using low values yields smaller dependencies on SO_2 for N_p and size: a value of 1×10^{-17} cm^3/s had N_p increase by about 50 % as Q_1 was increased from 8 to 50 sccm while a rate coefficient of 1×10^{-18} cm^3/s had a 22 % increase. Increasing this rate coefficient to 1×10^{-16} cm^3/s had large effects: as Q_1 varied from 8 to 50 sccm, particle size roughly doubled and N_p increased by an order of magnitude. A value of the order of 10^{-16} cm^3/s along with generation of OH in the reaction is probably the limit for simulations to remain congruent with the data. On the other hand, if a wall loss for HO_2 is significant in the experiment, much larger values for the rate coefficient would be needed in the simulations for the reaction to have significant effects.

Alternative explanations for an SO_2 dependence include uncertainties in HONO concentrations as well other clustering reactions. More HONO in the flow exiting the source and a smaller first-order photolysis rate is possible and this would likely result in predicted Np to have bigger changes with SO_2. SO_2 may react with oxidants within the small particles, leading to their growth.